ACS APPLIED MATERIALS & INTERFACES

Research Article

www.acsami.org

Mapping a Plasmonic Hologram with Photosensitive Polymer Films: Standing versus Propagating Waves

Thomas Papke,[†] Nataraja Sekhar Yadavalli,[†] Carsten Henkel,[‡] and Svetlana Santer*[,†]

[†]Department of Experimental Physics, Institute of Physics and Astronomy, University of Potsdam, 14476 Potsdam, Germany

[‡]Department of Quantum Optics, Institute of Physics and Astronomy, University of Potsdam, 14476 Potsdam, Germany

Supporting Information

ABSTRACT: We use a photosensitive layer containing azobenzene moieties to map near-field intensity patterns in the vicinity of nanogrids fabricated within a thin silver layer. It is known that azobenzene containing films deform permanently during irradiation, following the pattern of the field intensity. The photosensitive material reacts only to stationary waves whose intensity patterns do not change in time. In this study, we have found a periodic deformation above the silver film outside the nanostructure, even if the latter consists of just one groove. This is in contradiction to the widely accepted viewpoint that propagating surface plasmon modes dominate outside nanogrids. We explain our observation based on an electromagnetic hologram formed by the constructive interference between a propagating surface plasmon wave and the incident light. This hologram contains a stationary intensity and polarization grating that even appears in the absence of the polymer layer.

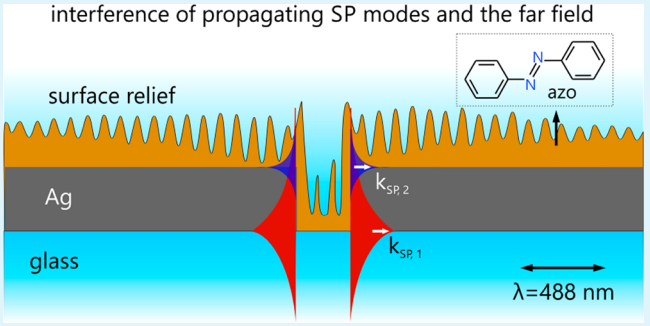

KEYWORDS: *propagating surface plasmons, nanostructured metal surface, azobenzene containing photosensitive material, surface relief grating*

1. INTRODUCTION

Azobenzene-containing photosensitive thin polymer films have attracted much attention in the last 20 years due to their peculiar response on light irradiation.[1−6] When exposed to irradiation with spatially varying distribution of intensity or polarization resulting from, for instance, the interference of two incoming beams, the photosensitive polymer film deforms according to the interference pattern and forms a surface relief grating (SRG).[7,8] At the heart of the SRG formation is the photoisomerization of the azobenzene molecule from *trans*- to *cis*-state accompanied by drastic changes in length, volume, and polarization of the molecule.[9,10] Under irradiation, the multiple trans to cis isomerizations result in a rotation of the azobenzene units that try to align their main axis perpendicular to the electrical field vector. This defines a p plane in places where the polarization is linear, and a preferred axis for circular or elliptic polarization. This induces a local ordering of the azobenzene molecules within the polymer matrix. Due to the coupling of the azobenzene molecules to the polymer matrix either via covalent bonding or through ionic interactions, the redistribution of the azobenzene molecules induces stresses within the polymer matrix. As a result, the film undergoes a viscoplastic deformation resulting in the formation of the SRG.[11−16] Although the mechanism of the SRG formation is not yet well understood,[17,18] the phenomenon has found a plenty of applications in a diverse areas such as in nano- and microsystem technology for surface patterning, photofluidization lithography and other photo alignment techniques.[2,19,20]

One of the interesting applications of the azobenzene polymer films is to use them as a "plaster cast" to map the irradiation properties, i.e., intensity and polarization distribution. Especially attractive here is the fact that the polymer film reacts to both far-field and near-field irradiation. The application of azobenzene polymers as a sensor for the near-field intensity distribution has several advantages over the conventional methods such as SNOM or two-photon photoemission electron microscopy (PEEM), namely, simplicity, absence of the complex experimental and analytical procedure and the possibility to imprint or "to freeze" the near-field intensity distribution in to the polymer topography. The latter in turn permits a detailed AFM analysis of the topography change and thus of the near-field distribution. Moreover, since the topography changes can be erased with irradiation or heating, one can reuse the same polymer-covered sample for multiple exposures and thus study the influence of, for instance, polarization, wavelength, and the intensity of the incoming light on the generated near-field intensity pattern.[21−26]

In this study, using photosensitive polymer material placed above a silver layer structured with one or several nanogrooves, we show that outside the nanogroove a standing near-field wave is generated during irradiation of the sample from the back side. Using analytical calculations, we explain this observation by the

Received: June 3, 2014
Accepted: July 21, 2014
Published: July 21, 2014

interference of propagating surface plasmon waves and the transmitted light resulting in a coherent plasmon hologram.

For the emerging fields of plasmonics and nanophotonics,[27] the understanding of the processes contributing to the total EM field at a distant point from the coupling structure such as nanometre scale grooves fabricated in metallic films[28−35] is one of the most fundamental but still controversial task.[36−39] Until now, the commonly accepted point of view is that near the nanogroove the scattering of the incident field into the SPP mode generates a propagating mode. Recently, it was experimentally shown using two-photon photoemission electron microscopy (PEEM) method, that near-field wave packets excited by 10 fs light pulses at a single groove fabricated in a thin silver film can interfere with the light incident at a 65° angle of incidence.[40] However, it is not clear whether the resulting electromagnetic field is a standing or propagating wave. In this article, we have elaborated this point.

2. EXPERIMENTAL METHODS

2.1. Fabrication of Nanogrids in a Metal Layer. A 60 nm thick silver layer was deposited on quartz glass (Hellma Optics, Germany) via PVD process using Univex 350 (Oerlikon Leybold Vacuum GmbH, Germany). The roughness of the metal layer was measured with tapping mode AFM (NTEGRA, NT-MDT, Russia) to be 3 nm (root-mean-square deviation). Nanogrooves of 200 nm in width and 60 nm in depth within the 60 nm thick Ag layer were fabricated using focused ion beam (FIB) lithography with a gallium-ion source (Zeiss AU-RIGA, Germany). The acceleration voltage, ion current, and etching time per line were chosen to be 30 kV, 20 pA, and 7 s, respectively.

2.2. Photosensitive Layer. In this study, we use as a photosensitive material, the azobenzene containing trimer shown in Figure 1c. The photosensitive material (trimer) is prepared by amide formation through the reaction of 1,3,5-benzenetricarbonyl trichloride (Alfa Aesar, 0.26 mmol) with *N*,*N*-dimethyl-4,4′-azodianiline (Aldrich, 0.78 mmol) in anhydrous dimethoxyethane (Aldrich) at room temperature in the presence of triethyl amine (Aldrich, 0.78 mmol) according to the described procedure.[41] A 40 nm thick photosensitive film is placed on top of the metal film with nanogrooves by spin coating of a dimethoxiethane trimer solution of c = 33 mg/mL concentration at 3000 rpm during 1 min. The thickness of the film was kept at 40 nm for all measurements. To determine the index of refraction of trimer, we have measured the UV−vis reflection and transmission spectra of 40 nm thin trimer film coated on glass substrate only. After measuring the spectra, the data was analyzed using APCSA (acceptance probability controlled simulated annealing) software, a method for modeling the optical constants of solids. The software fits a theoretical model for the reflection and transmission data using the transfer-matrix-method.[42] The material and geometrical parameters are determined by multiparameter minimization of the difference between theoretical and experimental values.[43,44] In this way, the complex refractive index of the photosensitive material (trimer) was determined to be $n_t = 1.94 + i0.27$ at a wavelength of λ_0 = 488 nm. The optical parameters of the Ag layer and quartz substrate at the wavelength λ_0 are $\varepsilon_{Ag} = -8.04 + i0.73$, and $\varepsilon_q = 2.13$, respectively.

2.3. Experimental Setup. To generate surface plasmon (SP) near fields, the metal nanogrooves covered with photosensitive trimer film were irradiated from the back side (glass side) with a horizontal linearly polarized (↔) laser beam of wavelength λ_0 = 488 nm (normal incidence) for 60 min (Figure 1a). The samples were positioned with the long axis of the nanogrooves perpendicular to the polarization direction. The intensity of the laser beam was kept constant for all experiments at I_0 = 100 mW cm^{-2}. The topography change in the trimer layer was afterward characterized using AFM in tapping mode. The optical parameters of the three layers (trimer/Ag/quartz) at the wavelength λ_0 are $\varepsilon_t = 3.69 + i1.05$ (trimer film), $\varepsilon_{Ag} = -8.04 + i0.73$ (silver), and $\varepsilon_q = 2.13$ (quartz substrate).

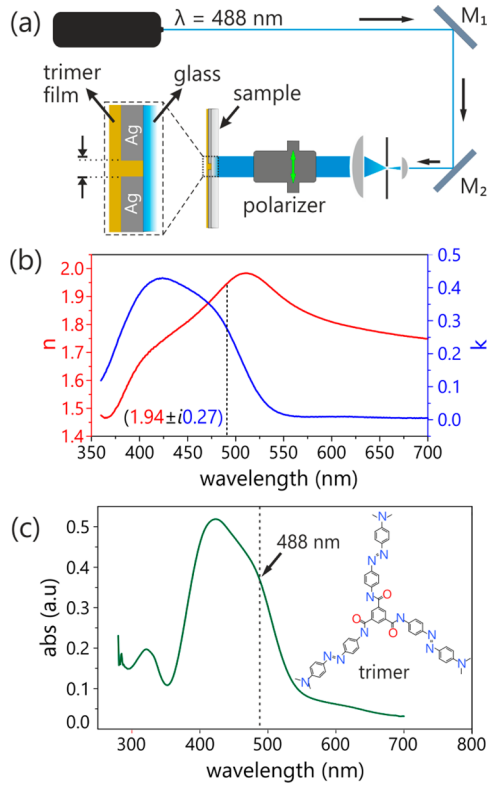

Figure 1. (a) Scheme of the optical setup: M_1, M_2, mirrors, a polarizer is used to control the polarization state of the beam. Green arrow represents the direction of transmission axis of the polarizer. (b) Refractive index of the photosensitive material (trimer) as a function of the wavelength. (c) UV−vis absorption spectra of trimer film. The inset shows the chemical structure of trimer.

3. RESULTS AND DISCUSSION

3.1. Plasmonic Hologram from a Single Nanogroove. The silver layer with a single nanogroove of 200 nm in width and 60 nm in depth (Figure 2a) was first covered with 40 nm thick photosensitive layer (in the following called trimer). The photosensitive material was adsorbed in the nanogroove resulting in its smaller depth of ca. 20 nm (Figure 2b). The roughness of the trimer layer was measured to be atomically flat with an RMS roughness of 0.4 nm over an area of 10 × 10 μm^2. After irradiation with the laser beam of wavelength λ_0 = 488 nm, the topography is deformed resulting in the formation of a surface relief grating (SRG) (Figure 2b).

A sinusoidal shaped SRG topography with a periodicity of d = (295 ± 5) nm appears on both sides of the nanogroove. The amplitude of this corrugation decays over a distance of approximately 10 μm, starting from 8 nm (peak to peak) near the groove down to the roughness of the trimer layer. A similar result is observed outside of nanogrids consisting of several nanogrooves (see Supporting Information 1 for detailed analysis). We find that the number of nanogrooves only influences the amplitude of the topographical relief, but not its periodicity, depth and propagation length. Since the photosensitive material reacts only to stationary holographic gratings, we are led to the conclusion that the nanogroove generates a standing near-field wave. This observation is in direct contradiction to the widely accepted point of view that the nanogroove generates *propagating* surface plasmon waves by scattering.[30,45,46] In the following, we elaborate on an explanation for our observation.

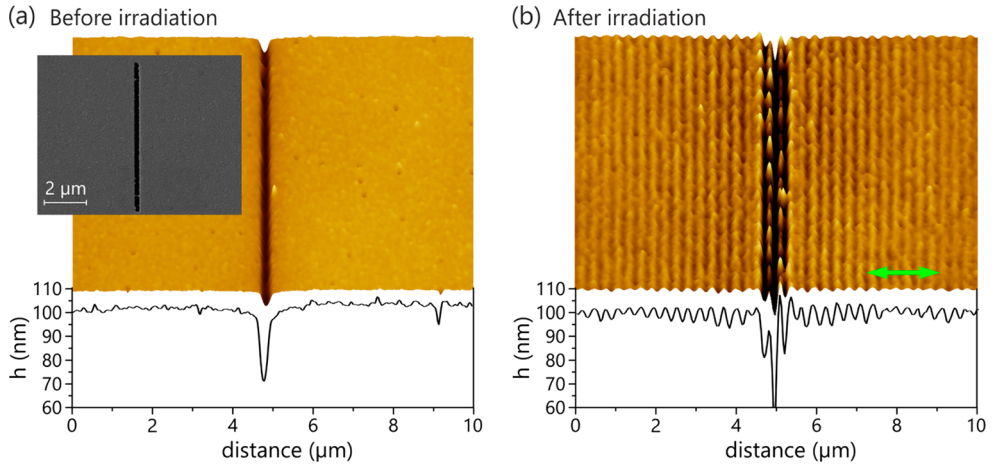

Figure 2. (a) AFM micrograph of a single nanogroove etched in the silver layer and covered with a 40 nm thick trimer layer, before irradiation. Inset: SEM micrograph of the bare silver topography with etched groove. (b) AFM micrograph at the same position after irradiation from the glass side with a laser beam (wavelength λ_0 = 488 nm) intensity of 5 mW/cm^2 for 60 min. Green arrow indicates the polarization of laser beam with respect the sample topography during irradiation.

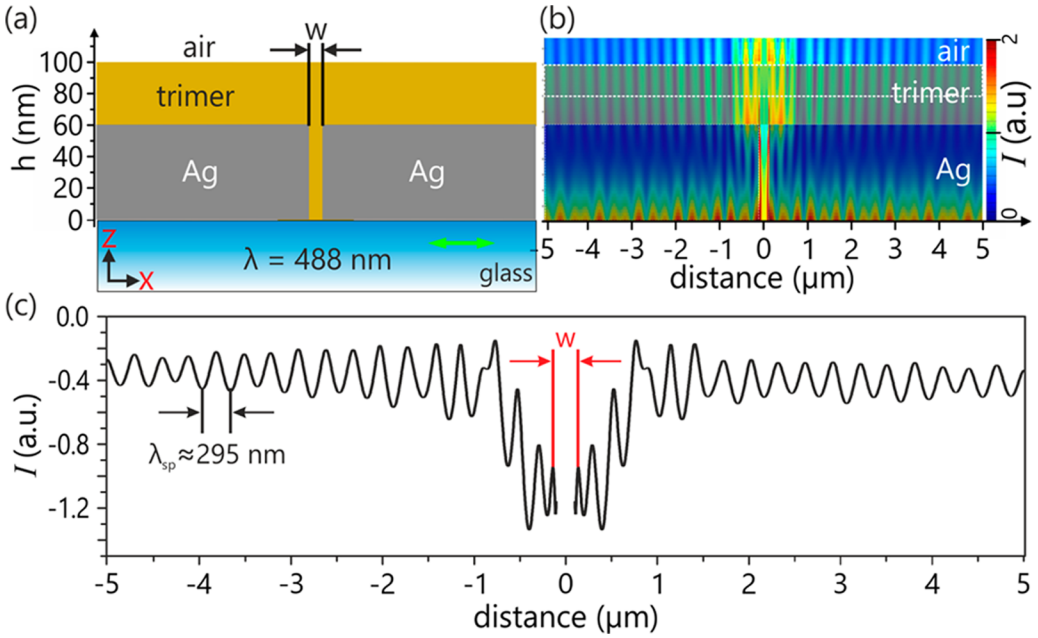

Figure 3. (a) Scheme of the sample structure used for the FDTD-simulation: the silver layer of 60 nm thickness is placed on a glass surface; a single nanogroove of 200 nm in width within the metal layer is covered with 40 nm thick layer of photosensitive material. (b) Simulated intensity distribution for a single nanogroove. (c) Cross section of the average intensity distribution in photosensitive material (area represented by white dotted box in (b).

3.2. FDTD Simulations. To investigate the near-field distribution in the vicinity of the nanogroove, we performed vectorial two-dimensional FDTD simulations (finite difference in the time domain, Lumerical Solution Inc.) for the sample geometry shown in Figure 3a. The size, geometry, and the optical parameters of the simulated nanogrooves are the same as in the experiment. A map of the field intensity around the nanogroove and a cross section through the trimer layer at mid-depth (20 nm below the surface) are shown in Figure 3, panels b and c, respectively. The abscissa is inverted, anticipating that the mass transport of the photosensitive material creates hills where the intensity is lower as it was shown earlier.[16] One can see that there is a high intensity at the border of the nanogroove that causes mass transport of the trimer out of the groove. The modulation of the intensity on both sides of the groove is reproduced with a period $\Lambda_{sp} \approx 295$ nm that closely matches the period d of the surface topography change (Figure 2b).

Also in the case of a nanostructure made from six nanogrooves, the results of the simulations are similar to the experimental observations. In Figure 4, we present two orthogonal nanogrids consisting of six nanogrooves each. After irradiation, the surface relief grating is observed only when the polarization direction of the incoming light is perpendicular to the main axis of the nanogrooves (grating B in Figure 4a). The corresponding FDTD simulations are shown in Figure 4(c,d). For grating A, the intensity is mostly localized in and between the grooves, with a very low level at the bottom of the trimer layer outside the nanogrooves. This situation is inverted for grid B where the intensity is localized at the bottom

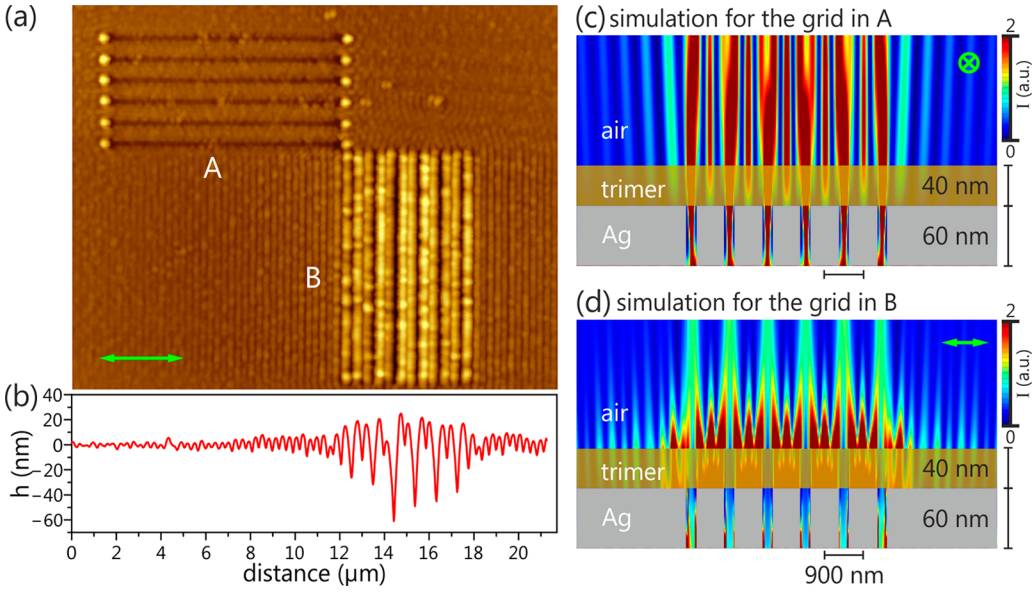

Figure 4. (a) AFM micrograph after 60 min irradiation with the wavelength of λ_0= 488 nm from the bottom of two orthogonal grids. The green arrow gives the polarization direction. (b) AFM cross section of the trimer topography in the vicinity of the grid B. (c) FDTD simulations of the intensity distribution for grid A (polarization parallel to the grooves) and (d) for grid B (polarization perpendicular to the grooves). For both nanogrids, periodicity, width, and depth of the nanogrooves are 900, 200, and 60 nm, respectively.

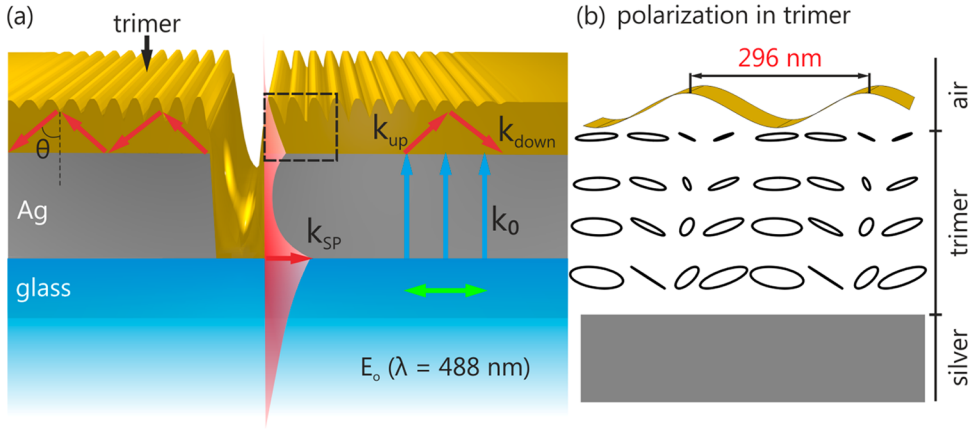

Figure 5. Visualization of plasmonic wave propagation in the photosensitive film. (a) Schematics of the waves that interfere in the layered structure: the incoming light (blue arrows) is scattered at the groove and generates a surface plasmon (red arrow and intensity profile) that penetrates by tunnelling into the photosensitive layer (two red arrows). The interference creates an intensity and polarization grating similar to a standing wave, but with a period $\Lambda_{sp} \approx 296$ nm given by the wavenumber of the lower-interface surface plasmon mode. (b) Illustration of the polarization structure in the holographic field: the ellipses and lines give the polarization (elliptic or linear), their size is proportional to the local electric field.

of the photosensitive layer, both between the nanogrooves and outside the nanogrid (Figure 4d). Note in particular the difference in the intensity patterns in the layer outside the nanostructure. This correlates with the formation of the SRG between and outside the nanogrooves observed in Figure 4a.

The topographical patterns between the nanogrooves show smaller pitches than the relief to the sides of the nanogrids. In the space between any two nanogrooves two topographical maxima were observed with a height of 18 nm. Since the trimer material goes into the intensity minima, the experimental results are in good agreement with the FDTD simulation where two minima of the near-field intensity between two nanogrooves are observed (Figure 4d). While the situation in between the nanogrooves is explained by standing waves resulting from the interference of two counter propagating SP waves generated in the nanogrooves as it was also reported by our group,[21,25] the structuring of the photosensitive material outside the nanogrid should be still clarified.

It is important to note that a SRG also forms outside the nanogrids when the polarization of the irradiation forms a 45° angle with the nanogrooves (for more details see Supporting Information 2). In this case, SP waves are generated by both nanogrids and lead to a topography in the form of a chessboard pattern. Note that a pattern of stripes would be expected from the interference of the two SP waves.

3.3. Surface Plasmon in the Layered System. To provide a more detailed picture of the optical field outside the nanogroove, we have performed calculations for the layered structure in order to identify its resonant modes.[47] This is based on the assumption that the wave field scattered by the nanogroove is particularly intense for those angles and frequencies that match resonances in the structure. These resonances are, for example, surface plasmons at the top and

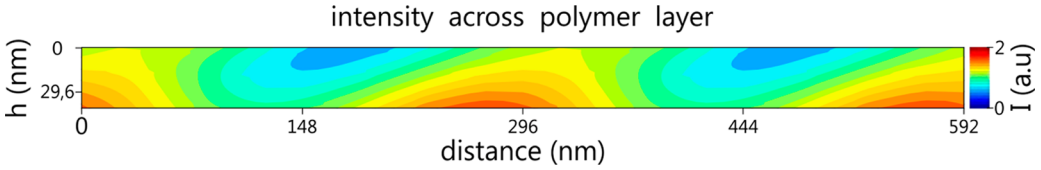

Figure 6. Intensity distribution in the photosensitive material from the air-interface into the material. Red color indicates maximum intensity.

bottom interface of the Ag film and waveguide modes in the trimer film. The wavelength Λ_{mt} of the surface plasmon mode at the top interface (metal−trimer) is given by[48]

$$\frac{1}{\Lambda_{mt}} = \frac{1}{\lambda_0} Re\sqrt{\frac{\varepsilon_{Ag}\varepsilon_d}{\varepsilon_{Ag}+\varepsilon_d}} \Rightarrow \Lambda_{mt} \approx 198\ \text{nm} \quad (1)$$

Where $\varepsilon_{Ag} = -8.04 + i0.73$ and $\varepsilon_d = 3.69 + i1.05$ are the permittivity of silver and trimer. For the quartz−metal interface, we have similarly, $\Lambda_{qm} \approx 287$ nm. Note that the wavelength of the surface plasmon at the *lower* interface matches better the periodicity of the topography measured experimentally. On the one hand, this could have been expected from the field map in Figure 3c where the field intensity is largest at the bottom of the metal film. On the other hand, one would expect an intensity modulation (and hence, a surface relief) at *half* the period of the surface plasmon mode.

Let us recall that eq 1 only describes a plasmon resonance at an infinitely thick metal layer (half-space). For the layer with a finite thickness, we have to work out how the field of the lower plasmon penetrates through the metal layer and couples into the trimer. This includes for example multiple reflections between the interfaces (see Figure 5). We have calculated the reflectivity of the layered structure and identified the resonant modes by dips as a function of the lateral wavenumber, in the spirit of the Kretschmann configuration.[44] This procedure yields a wavelength $\Lambda_{sp} \approx 296$ nm for our geometry, only slightly shifted from from the number $\Lambda_{qm} \approx 287$ nm given above. The resonant mode is actually extended throughout the metal into the photosensitive layer where it resembles a surface plasmon mode. (See the qualitative sketch of the mode intensity in Figure 5). Actually, we find that in the top layer, the mode is composed by two running waves that propagate up and down, undergoing total internal reflection at the trimer-air interface. These waves are forming an angle Θ with the normal given by

$$\Theta = \arcsin\frac{\lambda_0}{\Lambda_{sp} n_t} \approx 60° \quad (2)$$

As illustrated in Figure 5, the photosensitive material is thus exposed to three fields: the two waves that are part of the resonant mode in the layer, and the electric field E_0 from the incident laser beam. The complex amplitude of the field $Re[\vec{E}(x,z)\ e^{-i\omega t}]$ is thus

$$\vec{E}(x,z) = E_0(z)\vec{e}_x + E_{sp}\, e^{2\pi i x/\Lambda_{sp}}(\vec{e}_x \cos\Theta \cos(k_{zd}z - \phi) - i\,\vec{e}_z \sin\Theta \sin(k_{zd}z - \phi)) \quad (3)$$

where $\vec{e}_x$ and $\vec{e}_z$ are unit vectors parallel and perpendicular to the metal−trimer interface, Θ is the angle defined in eq 2, and $\pm k_{zd}$ are the vertical wave vector components of the two waves that form the resonant mode in the trimer layer (amplitude E_{sp}). The angle 2ϕ is the phase of the total internal reflection coefficient at the trimer-air interface. The illuminating laser has a field $E_0(z)$ which is weakly dependent on the depth z due to partial reflections at the interfaces.

The time-averaged intensity of this field contains a standing wave with period Λ_{sp} from the interference $E_0^* E_{sp}$ term between the two fields pointing along the unit vector $\vec{e}_x$ (see contour map in Figure 6). In addition, a polarization grating appears, as visualized in Figure 5b: the electric field vector lies in the plane of the figure (xz-plane) and traces out a more or less elongated ellipse over one period. The size of the ellipses illustrates the field intensity, and their shape the polarization state (linear or elliptic). The surface relief (top curve) has been added to the figure following previous investigations of the photomechanical response to a polarization grating: valleys correspond to regions of circular polarization.[16] For this calculation, we have assumed a fixed relative amplitude E_{sp} of the resonant plasmon mode relative to the incident laser. This is expected for the scattering of a coherent field at a stationary structure.

The upshot of this analysis is the existence of a stationary intensity and polarization grating with just the right period (Λ_{sp}) as observed experimentally: the plasmon mode that resonates in the layered structure interferes coherently with the exciting homogeneous beam, similar to the pulsed experiment of ref 40. The nanogroove acts as a scattering source for this resonant plasmon mode which therefore appears in the photosensitive layer on both sides of the groove. The interference (both in intensity and polarization) depends on a fixed phase relation between the incident and scattered fields and would disappear if the scattering were inelastic or incoherent. We thus attribute the topographical relief to the response of the photosensitive material to the coherent plasmon hologram created by this interference. If multiple grooves act as scatters, their spacing and number changes the efficiency of the scattering, similar to a resonant antenna, but not the period of the resonant plasmon mode, in agreement with the experimental results. Finally, we note that the appearance of the plasmonic hologram does not depend on the presence of the photosensitive material that influences only the value of Λ_{sp}. We have found that also in the case of a metal/air interface, a stationary electromagnetic wave results from the interference of the near-field wave generated by the nanogroove with the incident light.

4. CONCLUSIONS

Here, we report on mapping the plasmonic near field in the vicinity of a nanostructured metal film, using a photosensitive layer coated above. We have found that during irradiation with normal incidence through the substrate, the polymer deforms resulting in surface relief gratings (SRG) not only between the nanogrooves, but also outside the structure. The periodicity (297 nm) and propagation length (up to 10 μm) of this deformation does not depend on the number of nanogrooves. While the SRG formation between the nanogrooves is known to be the result of interference of two counter propagating waves generated in at the grooves, the topography outside the

nanogrooves was puzzling. Indeed, it is known that the polymer can be deformed only in the presence of a standing wave where local intensity patterns are spatially fixed. We provided a theoretical explanation for the experimental observation based on the constructive interference (plasmonic hologram) between a propagating surface plasmon modes and the incident light. We have argued that the photosensitive material influences only the wavelength of the hologram, which would also appear in the absence of the polymer layer.

■ ASSOCIATED CONTENT

Supporting Information

The dependence of plasmonic hologram length on number of nanogrooves and a chess board style multiple wave interference pattern resulting from two orthogonal grids are presented in Figures S1−S3. This material is available free of charge via the Internet at http://pubs.acs.org.

■ AUTHOR INFORMATION

Corresponding Author

*E-mail: santer@uni-potsdam.de.

Notes

The authors declare no competing financial interest.

■ ACKNOWLEDGMENTS

We would like to acknowledge Prof. Dr. Sc. Oleg Vyvenko and Dr. Yuri Petrov from the Interdisciplinary Resource Center for Nanotechnology (St. Petersburg, Russia) for their valuable support to use the advanced Zeiss Supra 40VP Scanning Electron Microscope. We thank Dr. Nino Lomadze for the synthesis of the trimer.

■ REFERENCES

(1) Zhao, Y.; Ikeda, T., Eds. *Smart Light-Responsive Materials: Azobenzene-Containing Polymers and Liquid Crystals*; Wiley: Hoboken, NJ, 2009.

(2) Priimagi, A.; Shevchenko, A. Azopolymer-Based Micro- and Nanopatterning for Photonic Applications. *J. Polym. Sci. Polym. Phys.* **2014**, *52*, 163−182.

(3) Seki, T.; Nagano, S.; Hara, M. Versatility of Photoalignment techniques: From Nematics to a Wide Range of Functional Materials. *Polymer* **2013**, *54*, 6053.

(4) Lee, S.; Kang, H. S.; Park, J.-K. Directional Photofluidization Lithography: Micro/Nanostructural Evolution by Photofluidic Motions of Azobenzene Materials. *Adv. Mater.* **2012**, *24*, 2069.

(5) Schuh, Ch.; Lomadze, N.; Ruhe, J.; Kopyshev, A.; Santer, S. Photomechanical Degrafting of Azo-Functionalized Poly(methacrylic acid) (PMAA) Brushes. *J. Phys. Chem. B* **2011**, *115*, 10431.

(6) Lomadze, N.; Kopyshev, A.; Ruhe, J.; Santer, S. Light-Induced Chain Scission in Photosensitive Polymer Brushes. *Macromolecules* **2011**, *44*, 7372−7323.

(7) Rochon, P.; Batalla, E.; Natansohn, A. Optically Induced Surface Gratings on Azoaromatic Polymer Films. *Appl. Phys. Lett.* **1995**, *66*, 136.

(8) Kim, D. Y.; Tripathy, S. K.; Li, L.; Kumar, J. Laser-Induced Holographic Surface Relief Gratings on Nonlinear Optical Polymer Films. *Appl. Phys. Lett.* **1995**, *66*, 1166.

(9) Saphiannikova, M.; Toshchevikov, V.; Ilnytsky, J. Nanoscopic Actuators in Light-Induced Deformation of Glassy Azo-Polymers. *Proc. SPIE* **2013**, *8901*, 890138.

(10) Toshchevikov, V.; Saphiannikova, M.; Heinrich, G. Light-Induced Deformation of Azobenzene Elastomers: A Regular Cubic Network Model. *J. Phys. Chem. B* **2012**, *116*, 913.

(11) Bian, S.; Li, L.; Kumar, J.; Kim, D. Y.; Tripathy, S. K. Single Laser Beam-Induced Surface Deformation on Azobenzene Polymer Films. *Appl. Phys. Lett.* **1998**, *73*, 1817−1819.

(12) Kumar, J.; Li, L.; Xiang, X. L.; Kim, D. Y.; Sung-Lee, T.; Tripathy, S. K. Gradient Force: The Mechanism for Surface Relief Grating Formation in Azobenzene Functionalized Polymers. *Appl. Phys. Lett.* **1998**, *72*, 2096−2098.

(13) Pedersen, T. G.; Johensen, P. M.; Holme, N. C. R.; Ramanujam, P. S.; Hvilsted, S. Mean-Field Theory of Photoinduced Formation of Surface Reliefs in Side-Chain Azobenzene Polymers. *Phys. Rev. Lett.* **1998**, *80*, 89−82.

(14) Bublitz, D.; Fleck, B.; Wenke, L. A Model for Surface-Relief Formation in Azobenzene Polymers. *Appl. Phys.* **2001**, *72*, 931−936.

(15) Yadavalli, N. S.; Santer, S. In-Situ Atomic Force Microscopy Study of the Mechanism of Surface Relief Grating Formation in Photosensitive Polymer Films. *J. Appl. Phys.* **2013**, *113*, 224304.

(16) Yadavalli, N. S.; Saphiannikova, M.; Lomadze, N.; Goldenberg, L. M.; Santer, S. Structuring of Photosensitive Material below Diffraction Limit using Far Field Irradiation. *Appl. Phys. A: Mater. Sci. Process.* **2013**, *113*, 263−272.

(17) Mechau, N.; Saphiannikova, M.; Neher, D. Molecular Tracer Diffusion in Thin Azobenzene Polymer Layers. *Appl. Phys. Lett.* **2006**, *89*, 251902.

(18) Juan, M. L.; Plain, J.; Bachelot, R.; Royer, P.; Gray, S. K.; Wiederrecht, G. P. Multiscale Model for Photoinduced Molecular Motion in Azo Polymers. *ACS Nano* **2009**, *3*, 1573.

(19) Lee, S.; Kang, H. S.; Park, J.-K. Directional Photofluidization Lithography: Micro/Nanostructural Evolution by Photofluidic Motions of Azobenzene Materials. *Adv. Mater.* **2012**, *24*, 2069−2103.

(20) Saphiannikova, M.; Toshchevikov, V.; Ilnytskyi, J. Photoinduced Deformations in Azobenzene Polymer Films. *Nonlinear Opt., Quantum Opt.* **2010**, *41*, 27−57.

(21) König, T.; Tsukruk, V.; Santer, S. Controlled Topography Change of Subdiffraction Structures Based on Photosensitive Polymer Films Induced by Surface Plasmon Polaritons. *ACS Appl. Mater. Interfaces* **2013**, *5*, 6009.

(22) König, T.; Sekhar, Y. N.; Santer, S. Surface Plasmon Nanolithography: Impact of Dynamically Varying Near-Field Boundary Conditions at the Air−Polymer Interface. *J. Mater. Chem.* **2012**, *22*, 5945−5950.

(23) König, T.; Santer, S. Stretching and Distortion of a Photosensitive Polymer Film by Surface Plasmon Generated Near Fields in the Vicinity of a Nanometer sized Metal Pin Hole. *Nanotechnology* **2012**, *23*, 155301.

(24) König, T.; Sekhar, Y. N.; Santer, S. Near-Field Induced Reversible Structuring of Photosensitive Polymer Films: Gold Versus Silver Nano-Antennas. *Plasmonics* **2012**, *7*, 535−542.

(25) König, T.; Santer, S. Visualization of Surface Plasmon Interference by Imprinting Intensity Patterns on a Photosensitive Polymer. *Nanotechnology* **2012**, *23*, 485304.

(26) König, T.; Goldenberg, L. M.; Kulikovska, O.; Kulikovsky, L.; Stumpe, J.; Santer, S. Reversible Structuring of Photosensitive Polymer Films by Surface Plasmon Near Field Radiation. *Soft Matter* **2011**, *7*, 4174.

(27) Lindquist, N. C.; Nagpal, P.; McPeak, K. M.; Norris, D. J.; Oh, S.-H. Engineering Metallic Nanostructures for Plasmonics and Nanophotonics. *Rep. Prog. Phys.* **2012**, *75*, 036501.

(28) Lee, K. G.; Park, Q.-H. Coupling of Surface Plasmon Polaritons and Light in Metallic Nanoslits. *Phys. Rev. Lett.* **2005**, *95*, 103902.

(29) Wuenschell, J.; Kim, H. K. Surface plasmon Dynamics in an Isolated Metallic Nanoslit. *Opt. Express* **2006**, *95*, 10000.

(30) Wang, B.; Aigouy, L.; Bourhis, E.; Gierak, J.; Hugonin, J. P.; Lalanne, P. Efficient Generation of Surface Plasmon by Single-Nanoslit Illumination under Highly Oblique Incidence. *Appl. Phys. Lett.* **2009**, *94*, 011114.

(31) He, M.-D.; Liu, J.-Q.; Wang, K.-J.; Wang, X.-J.; Gong, Z.-Q. Efficient Directional Excitation of Surface Plasmon Polaritons by Partial Dielectric Filling Slit Structure. *Opt. Commun.* **2012**, *285*, 4588.

(32) Kihm, H.-W.; Kihm, Q. H.; Kim, D. S.; Ahn, K. J.; Kang, J. H. Phase-Sensitive Imaging of Diffracted Light by Single Nanoslits: Measurements from Near to Far Field. *Opt. Express* **2010**, *18*, 15725.
(33) Ung, B.; Sheng, Y. Interference of Surface Waves in a Metallic Nanoslit. *Opt. Express* **2007**, *15*, 1182.
(34) Jung, Y. S.; Wuenschell, J.; Schmidt, T.; Kim, H. K. Near- to Far-Field Imaging of Free-Space and Surface-Bound Waves Emanating from a Metal Nanoslit. *Appl. Phys. Lett.* **2008**, *92*, 023104.
(35) Kim, H.; Lee, B. Unidirectional Surface Plasmon Polariton Excitation on Single Slit with Oblique Backside Illumination. *Plasmonics* **2009**, *4*, 153.
(36) Gay, G.; Alloschery, O.; Viaris de Lesegno, B.; O'Dwyer, C.; Wainer, J.; Lezec, H. J. The Optical Response of Nanostructured Surfaces and the Composite Diffracted Evanescent Wave Model. *Nat. Phys.* **2006**, *2*, 262−267.
(37) Garcia-Vidal, F. J.; Rodrigo, S. G.; Martin-Moreno, L. Foundations of the Composite Diffracted Evanescent Wave Model. *Nat. Phys.* **2006**, *2*, 790.
(38) Weiner, J.; Lezec, H. J. Reply: Foundations of the Composite Diffracted Evanescent Wave Model. *Nat. Phys.* **2006**, *2*, 791.
(39) Lalanne, P.; Hugonin, J. P.; Besbes, M.; Bienstman, P. Reply: The Response of Nanostructured Surfaces in the Near Field. *Nat. Phys.* **2006**, *2*, 792−793.
(40) Zhang, L.; Kubo, A.; Wang, L.; Petek, H.; Seideman, T. Imaging of Surface Plasmon Polariton Fields Excited at a Nanometer-Scale Slit. *Phys. Rev. B* **2011**, *84*, 245442.
(41) Goldenberg, L. M.; Kulikovsky, L.; Kulikovska, O.; Tomczyk, J.; Stumpe, J. Thin Layers of Low Molecular Azobenzene Materials with Effective Light-Induced Mass Transport. *Langmuir* **2009**, *26*, 2214−2217.
(42) Harbecke, B. Coherent and Incoherent Reflection and Transmission of Multilayer Structures. *Appl. Phys. B: Laser Opt.* **1986**, *39*, 165−170.
(43) Djurisic, A. B.; Fritz, T.; Leo, K. Determination of Optical Constants of Thin Absorbing Films from Normal Incidence Reflectance and Transmittance Measurements. *Opt. Commun.* **1999**, *166*, 35−42.
(44) Rakic, A. D.; Elazar, J. M.; Djurisic, A. B. Acceptance-Probability-Controlled Simulated Annealing: A Method for Modeling the Optical Constants of Solids. *Phys. Rev. E* **1995**, 52.
(45) Rotenberg, N.; Spasenovic, M.; Krijger, T. L.; le Feber, B.; Garcia de Abajo, F. J.; Kuipers, L. Plasmon Scattering from Subwavelength Holes. *Phys. Rev. Lett.* **2012**, *108*, 127402.
(46) Kuttge, M.; Garcia de Abajo, F. J.; Polman, A. How Grooves Reflect and Confine Surface Plasmon Polaritons. *Opt. Express* **2009**, *17* (12), 10385.
(47) Yeh, P. *Optical Waves in Layered Media*; J. Wiley & Sons: New York, 1988.
(48) Raether, H. *Surface Plasmons on Smooth and Rough Surfaces and on Gratings*; Springer Tracts in Modern Physics: Berlin, 1988.